Electrical Power and Energy Systems 147 (2023) 108804

Contents lists available at ScienceDirect

International Journal of Electrical Power and Energy Systems

journal homepage: www.elsevier.com/locate/ijepes

Extended real-time voltage instability identification method based on synchronized phasor measurements

Alan P.F. Ferreira [a,c,*], Denis Osipov [b], Glauco N. Taranto [c], Tatiana M.L. Assis [c], Joe H. Chow [b]

[a] Department of Electrical Engineering, Federal Center for Technological Education of Rio de Janeiro, Rio de Janeiro 28635-080, Brazil
[b] Department of Electrical, Computer, and Systems Engineering, Rensselaer Polytechnic Institute, Troy, NY 12180, USA
[c] Department of Electrical Engineering, Federal University of Rio de Janeiro - COPPE, Rio de Janeiro 21945-970, Brazil

ARTICLE INFO

Keywords:
Phasor measurements
Real-time estimation
Thévenin equivalent
Voltage stability assessment

ABSTRACT

This paper presents an extended adaptive approach designed to accurately estimate the Thévenin equivalent parameters using phasor measurements at a given bus for measurements lying in any of four quadrants of the PQ-plane. The improvement is achieved by using a new condition to properly update the estimated parameters after an initial guess. Based on an adaptive philosophy, the proposed approach can correctly account for the intrinsic nonlinearities of a power system, can provide a real-time estimation of Thévenin parameters, and does not require network topology knowledge. The method is validated using the Kundur 2-area system, showing estimation improvements compared to the current adaptive approach and the classical recursive least-squares method. The proposed approach is able to estimate both sides of the system with respect to the measurement bus. In addition, a data-driven voltage stability index is developed. To illustrate the performance of the proposed approach in a larger power system, a voltage stability assessment is carried out on the IEEE 39-bus system, considering the action of overexcitation limiters of generators and nonlinear loads. The proposed approach is suitable for applications that require an accurate Thévenin equivalent estimation in real-time, such as for voltage stability assessment. The new approach provides a reliable tool for the system operators to make proper and timely decisions.

1. Introduction

The fast pace of new renewable energy resources (RER) installation (18 months), compared to new transmission lines construction (6 years), compounded by escalating electricity demand [1] and likely growth of power supply disruptions due to extreme events [2], may lead the existing transmission infrastructure to operate closer to its voltage stability limits [3,4]. This condition threatens secure system operation [5,6], and as a result, the development of online strategies to monitor the onset of voltage instability is kept at a high priority status on the power system research agenda [7].

A way to address real-time voltage stability assessment (VSA) is to take advantage of the phasor measurement unit (PMU) infrastructure that has been expanding throughout power systems around the globe, a fact that has inspired many applications toward the monitoring, protection, and controls in interconnected power grids [8,9]. An important benefit of using PMUs measurements for real-time analysis is its fast-sampling rate of 30 to 60 measurements per second, when compared with other large-scale digital measurements, such as from SCADA systems, where each update takes 2 to 5 s [10].

Specifically concerning VSA, reference [5] provides a survey containing strategies intended to detect the voltage instability onset, either for local or wide-area monitoring and considering the use of synchronized measurements. Among the given possibilities is the use of Thévenin equivalent-based models, adopted throughout this work to tackle the issue of assessing voltage stability in power systems.

The employment of Thévenin equivalent-based models targets to represent the behavior of an external system, seen from a given electric node (bus), by a voltage source in series with an impedance, known as Thévenin voltage ($\overline{E}_{Th}$) and Thévenin impedance ($\overline{Z}_{Th}$), respectively [11,12]. Fig. 1 shows a Thévenin equivalent circuit connected to a load bus. The use of this simple model enables a variety of applications in power systems, including but not limited to short-circuit current computation, fault location, electromagnetic transient studies, as well as VSA [12], the focus of this work.

The main idea of the approach is to accurately compute the equiv-

* Corresponding author at: Department of Electrical Engineering, Federal Center for Technological Education of Rio de Janeiro, Rio de Janeiro 28635-080, Brazil.
E-mail address: alan.ferreira@cefet-rj.br (A.P.F. Ferreira).

https://doi.org/10.1016/j.ijepes.2022.108804
Received 12 July 2022; Received in revised form 1 October 2022; Accepted 13 November 2022
Available online 29 November 2022

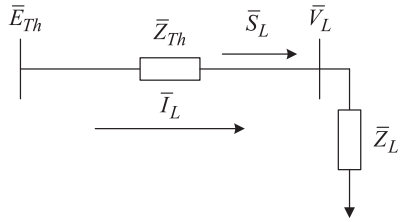

Fig. 1. Thévenin equivalent from a load bus.

alent parameters ($\bar{E}_{Th}$ and $\bar{Z}_{Th}$) from the buses of interest, keep the parameters updated as fast as possible to track topological changes, and monitor the maximum power transfer (MPT) constrained by the voltage stability limit of the system [4,13].

From the literature, it is possible to define classes of methods for VSA [14]: those based on measurements and network topology (the model-based methods [14,15]), and methods solely based on measurements (the measurement-based methods [16]- [17]), where the topology information is not required, which is the approach adopted in this paper.

The PMU-based VSA approach in [16], from this point, also referred to as the adaptive approach, has many advantages: representation of the effects of nonlinearities due to control actions [18,19]; the absence of a requirement of phase drift corrections due to slip between system frequency and PMU sampling frequency [11], as required in [20]; the absence of a requirement of network topology knowledge, as required in [15] and [14]; providing similar accurate estimation as if all models are known [21]; and finally, its characteristic of real-time estimation, requiring a time window of just two measurements to update its parameters [16].

However, evaluating the formulations and assumptions made by the authors in [16], confirmed by simulations results described in Section 4, one can show that this approach is not able to properly estimate the Thévenin parameters when the PMU measurements correspond to loads with a leading power factor, or if the load change between two consecutive measurements happens with varying power factor.

These drawbacks may limit the employment of this approach in some applications, for example, where the load is not directly connected to the evaluated bus (e.g., for a transit bus), or when the evaluated bus is subjected to the actions of distributed energy resources, which can render the active and reactive powers having a bidirectional behavior for some periods of time. As a result, despite all the favorable features, the adaptive approach may provide inaccurate estimations in such contexts either for the Thévenin parameters or the voltage stability limits.

Looking to fill the gaps left by the adaptive approach, but still taking advantage of its features, this work proposes an extension of [16,18], enabling the new approach to provide proper estimations for loading conditions in any of the four quadrants of the *PQ*-plane (Fig. 2), without the requirement of constant power factor load variation between two consecutive samples. As a result, the proposed extended adaptive approach makes possible the estimation in both directions of active power flow with respect to a boundary bus, as illustrated in Fig. 3, which is an improvement compared to the recursive least-squares filter [11].

The contributions of this paper include:

1) Improvement of the Thévenin parameters updating criteria employed by the current adaptive approach [16] to provide proper estimations of the Thévenin equivalent in real-time, considering measurements lying in any of the four quadrants of the PQ-plane, Fig. 2, which is a condition not addressed in [16]. These actions add robustness to the extended version of the approach.
2) Development of an algorithm to consistently correct the estimated Thévenin parameters at any power system bus (a load, a transit bus, etc.), using two consecutive PMU measurements.
3) The derivation of a data-driven voltage stability index based only on local measurements of active power and current magnitude, aiming to improve situational awareness with respect to voltage stability.

2. Proposed approach

This section describes the theoretical basis for the proposed approach.

The Thévenin equivalent seen from a load bus is shown in Fig. 1, where $\bar{E}_{Th} = E_{Th}\angle\beta$ is the Thévenin voltage phasor, $\bar{Z}_{Th} = R_{Th} + jX_{Th}$ the Thévenin impedance, $\bar{I}_L = I_L\angle 0$ the load current phasor, $\bar{V}_L = V_L\angle\theta$ the load voltage phasor, $\bar{Z}_L = Z_L\angle\theta$ the load impedance, θ the angle between the load voltage and the load current, and β the angle between the Thévenin voltage and the load current. Applying Kirchhoff's voltage law to the circuit in Fig. 1, the Thévenin voltage can be described as

$$\bar{E}_{Th} = \bar{Z}_{Th}\bar{I}_L + \bar{V}_L \tag{1}$$

From the perspective of high-voltage transmission-level buses, $X_{Th} >> R_{Th}$. Hence, the assumption of $R_{Th} \approx 0$ becomes feasible making it possible to set $\bar{Z}_{Th} = jX_{Th}$. Then, separating (1) into its real and imaginary components results in

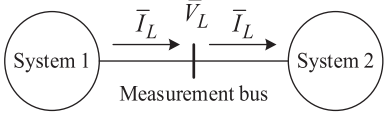

Fig. 3. Measurement bus separating two systems.

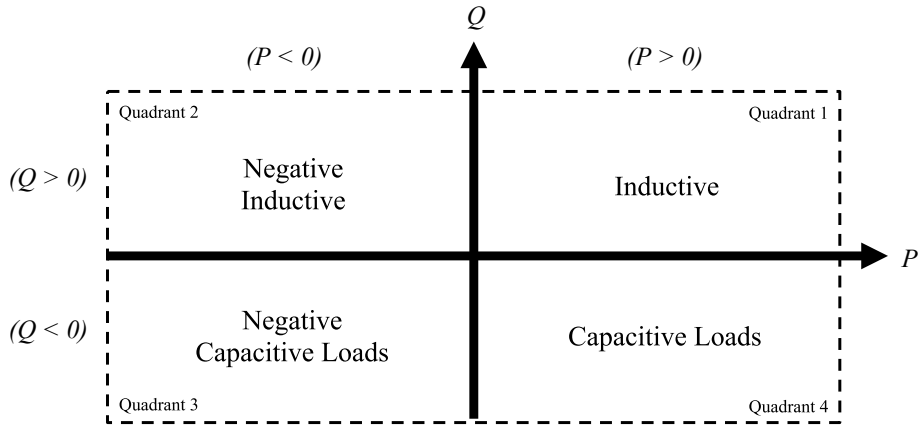

Fig. 2. Four quadrants corresponding to active and reactive power signs.

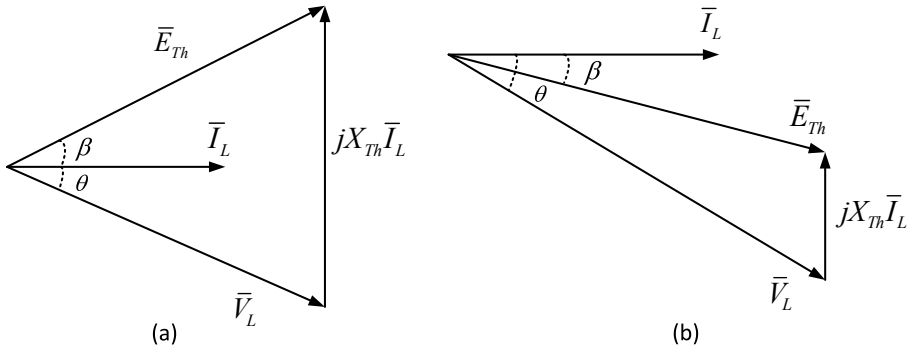

Fig. 4. Phasor diagram for capacitive loads: (a) positive β and (b) negativeβ.

$$\begin{pmatrix} E_{Th}\cos\beta = V_L\cos\theta \\ E_{Th}\sin\beta = X_{Th}I_L + V_L\sin\theta \end{pmatrix} \tag{2}$$

In (2) I_L, V_L, and θ are known from measurements, whereas E_{Th}, X_{Th}, and β are unknown.

2.1. The adaptive approach

To solve the underdetermined system (2) the authors in [16] set E_{Th} as a free variable, which means that an initial guess is specified for E_{Th}, and then the other unknowns (X_{Th} and β) are computed using (3) and (4), derived from (2), as

$$\beta = \arccos\left(\frac{V_L\cos\theta}{E_{Th}}\right) \tag{3}$$

$$X_{Th} = \frac{E_{Th}\sin\beta - V_L\sin\theta}{I_L} \tag{4}$$

If the actual value is chosen for E_{Th}, then X_{Th} and β will achieve their correct values as well.

The criterion to choose the initial guess for E_{Th} is to set it equal to the average value (E_{Th}^{avg}) between the minimum ($E_{Th}^{\min}$) and maximum ($E_{Th}^{\max}$) possible values for the Thévenin voltage from the base case condition.

$$E_{Th}^{\min} = V_L^0, \quad E_{Th}^{\max} = \frac{V_L^0\cos\theta^0}{\cos\beta^{\max}} \tag{5}$$

where $\beta^{\max}$ is the value of β when MPT takes place, i.e., when $X_{Th} = Z_L$, which is given by $\beta^{\max} = \arctan\left(\frac{Z_L^0 I_L^0 + V_L^0\sin\theta^0}{V_L^0\cos\theta^0}\right)$. The superscript "0″ refers to the quantities from the initial guess.

To bring E_{Th} from its initial guess towards the actual value, increments or decrements are performed depending on whether the E_{Th} guess is under- or over-estimated, respectively, for every new available PMU measurement that forms a new pair of measurements. To drive this decision in each step, a theorem developed by the authors in [16], based on the variation of the absolute value of the load impedance ΔZ_L, and the difference ΔX_{Th} between two consecutive estimated values for the Thévenin reactance using (4) is employed. The following actions are carried out by the adaptive approach:

1) If $\Delta X_{Th}^i \cdot \Delta Z_L^i > 0$, then E_{Th}^{i-1} is overestimated
   - Action: Decrease E_{Th}^i, i.e., $E_{Th}^i = E_{Th}^{i-1} - \Delta E_{Th}^i$;
2) If $\Delta X_{Th}^i \cdot \Delta Z_L^i < 0$, then E_{Th}^{i-1} is underestimated
   - Action: Increase E_{Th}^i, i.e., $E_{Th}^i = E_{Th}^{i-1} + \Delta E_{Th}^i$
3) If $\Delta X_{Th}^i = 0$ or $\Delta Z_L^i = 0$
   - Action: $E_{Th}^i = E_{Th}^{i-1}$

where "i" refers to the new measurement, "$i-1$" refers to the previous one, $\Delta Z_L^i = Z_L^i - Z_L^{i-1}$, and $\Delta X_{Th}^i = X_{Th}^i - X_{Th}^{i-1}$ are the load and estimated Thévenin reactance variations, respectively. The increment $\Delta E_{Th}^i = |E_{Th}^{i-1} \cdot k_a|$ is applied once the updating direction is known (increment or decrement). According to [16], the recommended value for k_a ranges from 0.0001 to 0.001. In short, the theorem increases E_{Th}^i when ΔZ_L and ΔX_{Th} have the same signs, and decreases E_{Th}^i when ΔZ_L and ΔX_{Th} have opposite signs. If $\Delta X_{Th}^i = 0$ the convergence is achieved, and $\Delta Z_L^i = 0$ means that the load impedance did not vary for the given interval.

2.2. Limitations of the current model

The issue of applying the adaptive approach to any bus of a power grid to assess the voltage stability, lies in the fact of its limitation to make accurate estimations only for Quadrant 1 in Fig. 2, i.e., for positive active and reactive power. Following, those issues are described:

1) Estimations for Quadrant 2 – Negative "P"

If the power measured at a bus belongs to Quadrant 2, e.g., due to the presence of RERs, the negative active power may yield $E_{Th}^{\max}$ with a negative value, according to (5). Thus, when E_{Th}^{avg} is computed as the initial guess for E_{Th} it may be out of the feasible range, and therefore, the adaptive approach may not converge.

2) Estimations on Quadrants 3 and 4 – Negative "Q"

If the measurements are in Quadrants 3 or 4, the issue is the reactive power being negative, i.e., with a capacitive characteristic. For those loading power factor conditions, β can be either positive or negative. Fig. 4 contains two phasor diagrams that illustrate each of these conditions.

From Fig. 4(b), one can verify that if $\bar{I}_L$ is small, $\bar{E}_{Th}$ may lag the reference phasor $\bar{I}_L$, resulting β having a negative value. In (3), a cosine function is employed to obtain β, implying $\beta > 0$. As a result, this formulation only provides the absolute value. An incorrect value of β would lead to erroneous X_{Th} and E_{Th}, leading to incorrect adjustments in the adaptive approach.

3) Load Power Factor Variation

As described in Section 2.1, the adaptive approach relies on a theorem that compares ΔZ_L and ΔX_{Th} to define corrections on the estimated Thévenin parameters. Nonetheless, this theorem is only reliable when the load power factor is kept constant for the two considered measurements. To further describe this situation, consider the two-bus system in Fig. 1, when the actual parameters are $E_{Th} = 1.0$ pu and $X_{Th} = 0.10$ pu. Two cases are considered.

To clarify the updating direction error happens due to power factor

Table 1
Performance Comparison of the approach in different conditions.

Case	$Z_{L1}(pu)$	$Z_{L2}(pu)$	$E_{Th0}(pu)$	$X_{Th1}(pu)$	$X_{Th2}(pu)$	$\Delta X_{Th}(pu)$	$\Delta Z_L(pu)$
1	0.90 + j0.18	0.45 + j0.09	1.0001	0.10032	0.10013	−1.92E-04	−0.45891
			0.9999	0.09968	0.09987	1.92E-04	−0.45891
2	0.90 + j0.18	0.81 + j0.09	1.0001	0.10032	0.10036	4.69E-5	−0.10284
			0.9999	0.09968	0.09964	−4.72E-05	−0.10284

Table 2
Computing ΔX_{Th} for over and underestimated..E_{Th}

Case #2	E_{Th0}(pu)	ΔE_{Th}(pu)	$E_{Th1}(pu)$	$X_{Th1}(pu)$	$X_{Th2}(pu)$	$\lvert\Delta X_{Th}\rvert(pu)$
Overestimated E_{Th}	1.0001	0.00005	1.00005 (decrement)	0.1001586	0.1001821	2.35E-05
			1.00015 (increment)	0.1004756	0.1005457	7.02E-05
Underestimated E_{Th}	0.9999	0.00005	0.99985 (decrement)	0.0995237	0.0994528	7.09E-05
			0.99995 (increment)	0.0998413	0.0998178	2.36E-05

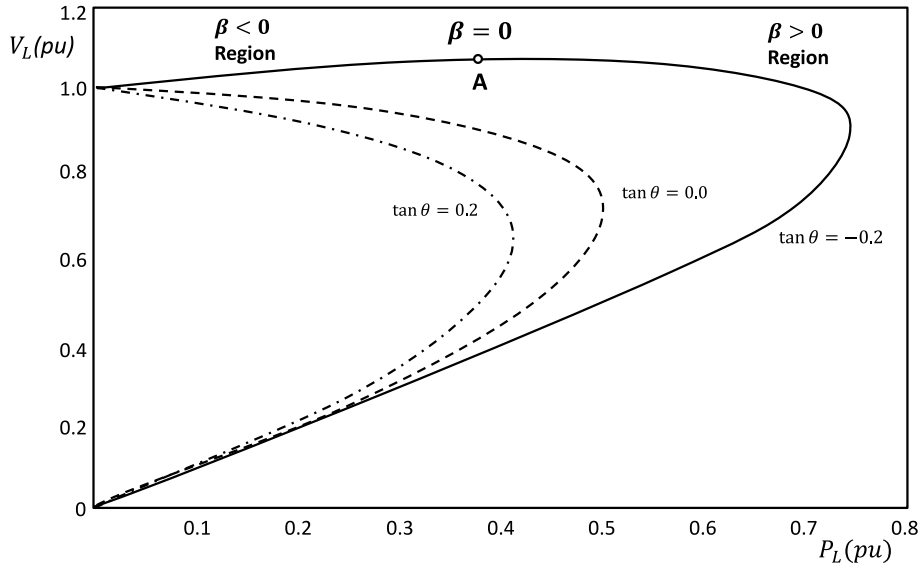

Fig. 5. Capacitive PV curve showing the negative and positive regions for β.

variation and not because of a possible large disturbance, in Case 1, the load impedance variation ΔZ_L is 50 % between the two consecutive measurements, and the power factor is kept constant. In Case 2, Z_L varies by 10.3 %, with R_L varying by 10 %, and X_L by 50 % between the two loading conditions; hence, the power factor is not kept constant. The theorem in [16] is tested for both cases with the initial guess of the Thévenin voltage either overestimated ($E^0_{Th} = 1.0001$ pu) or underestimated ($E^0_{Th} = 0.9999$ pu), as shown in Table 1.

For Case 1, one can verify that the theorem described in Section 2.1 works properly, since ΔX_{Th} and ΔZ_L have the same signs when E^0_{Th} is overestimated, and opposite signs when it is underestimated. Several other similar cases have been tested considering different step changes on Z_L but keeping the same power factor. For all those tests the adaptive approach theorem works correctly.

However, in Case 2, the theorem fails to provide the proper updating directions, since for the overestimated scenario ΔX_{Th} and ΔZ_L have opposite signs, and for the underestimated scenario they have the same signs, i.e., the theorem indicates to increase E_{Th} when it should be decreased and vice-versa. It is timely to mention that the above theorem may work for some cases of not constant power factor, but it is not the rule. A succession of wrong updates may happen, leading the Thévenin parameters estimation to diverge from the actual values and providing an inaccurate evaluation of Thévenin-based power margin indexes. Appendix A shows the comparison between the result from the simplified formulation employed in [16] to prove the theorem, and the result from the equation without simplification.

Thus, relying on the comparison of ΔX_{Th} and ΔZ_L to adaptively update the estimated Thévenin parameters towards the actual quantities have shown to be ineffective when ΔZ_L comes from two loading conditions with different power factors.

2.3. Sufficient condition for Thévenin parameters corrections

As illustrated in Table 1, the update conditions in [16] are not sufficiently comprehensive to account for non-constant power factor cases, and the derivations described in Appendix A.2 show why those conditions may fail.

Instead of just relying on whether E_{Th} is over- or under-estimated, one can use the fact that when $\Delta X_{Th} = 0$, the convergence is achieved, i.e., all estimated Thévenin parameters are equal to the actual values. Thus, regardless of whether ΔX_{Th} is a positive or a negative value, the key information is when its absolute value is closer to zero.

From that aspect, the proposed approach aims to minimize the absolute value of ΔX_{Th}, namely $|\Delta X_{Th}|$, from consecutive updates of the estimated E_{Th} for every new available set of measurements, i.e., E_{Th} should be decreased or increased in such a way the value computed for $|\Delta X_{Th}|$ becomes smaller than in the previous step, which will reflect the convergence of E_{Th} and X_{Th} to their actual values.

Compared to Table 1 using the method in [16], Table 2 shows the results obtained by the extended adaptive method. Here $|\Delta X_{Th}|$ is computed for the over and underestimated values of E_{Th} for Case #2. Considering an update size of $\Delta E_{Th} = 0.00005$ pu, one can verify that in both cases $|\Delta X_{Th}|$ decreases when the correct updating direction is performed, i.e., when a decrement is chosen for the overestimated occurrence, and when an increment for the underestimated one. E_{Th1} is the updated value from the initial guess value E_{Th0}, i.e., $E_{Th1} = E_{Th0} \pm \Delta E_{Th}$.

In this way, it is possible to state that the minimization of $|\Delta X_{Th}|$ can bridge the gap in the condition to compare ΔX_{Th} and ΔZ_L from the adaptive approach, being the sufficient condition to properly update the Thévenin parameters, regardless of power factor variation, disturbance magnitude, and *PQ*-plane quadrants.

2.4. Negative β detection approach

Negative values of β are possible when the equivalent load has a capacitive effect, namely in Quadrants 3 and 4 of Fig. 2. However, a capacitive load characteristic does not mean that β is always negative, a condition that usually is related to low values of X_{Th} and/or light loading conditions on the network, as shown by the phasor diagram in Fig. 4(b), making $\overline{E}_{Th}$ lagging $\overline{I}_L$.

In Section 2.2.2 it is shown that the formulation (3), to compute β, is unable to provide negative values when the actual β is negative, since arccosine is an even function. To address this issue, consider the perspective of the Thévenin equivalent voltage source $\overline{E}_{Th}$ in Fig. 1. If $\overline{E}_{Th}$ lags $\overline{I}_L$, then the total impedance $\overline{Z}_{total}$ seen by $\overline{E}_{Th}$ is capacitive. The total system impedance $\overline{Z}_{total}$ is given by

$$\overline{Z}_{total} = (R_L + jX_L) + jX_{Th} = R_{total} + jX_{total} \tag{6}$$

As X_L is negative for capacitive loads, in order for $\overline{Z}_{total}$ to become capacitive, $|X_L|$ needs to be greater than X_{Th}, since the equivalent transmission system X_{Th} is inductive. For inductive load cases, both X_L and X_{Th} are positive values, and thus $\overline{Z}_{total}$ always has an inductive characteristic, meaning that β is always positive as well.

To visualize conditions when β is negative, consider the *PV*-plot in Fig. 5, consisting of three loading conditions: a resistive load ($\tan\theta = 0$), an inductive load ($\tan\theta = 0.2$), and a capacitive load ($\tan\theta = -0.2$).

For the capacitive load curve (solid line), one can verify that the load voltage V_L increases as the load active power P_L increases, peaking at point A. From the initial loading condition ($P_L = 0$) to the loading condition A ($P_L \approx 0.38$ pu), the load power is sufficiently low to keep its impedance high enough to make $|X_L| \rangle X_{Th}$, Fig. 4(a), where $\overline{E}_{Th}$ lags $\overline{I}_L$. During this interval $\overline{Z}_{total}$ is capacitive, thus making β negative, which is pointed out over the solid curve in Fig. 5. As a capacitive load creates a negative voltage drop along the circuit, the voltage increases as P_L increases.

At point A, the voltage peak on the solid curve reflects that $|X_L| = X_{Th}$, meaning the reactive power consumed by the transmission network is equal to the reactive power provided by the capacitive load, and $\overline{E}_{Th}$ and $\overline{I}_L$ are in phase for this condition. After this point, $|X_L| \langle X_{Th}$, which happens in a heavy loading scenario, and the voltage starts to drop because now $\overline{Z}_{total}$ becomes inductive, meaning that the voltage drop is positive with positive β, Fig. 4(b), where $\overline{E}_{Th}$ leads $\overline{I}_L$.

Thus, one can verify that the sign of β is directly related to the values of $|X_L|$, X_{Th}, and X_{total}. From the 2-bus system in Fig. 1, for the condition where $R_{Th} = 0$, the magnitude of the load voltage V_L is

$$V_L = \frac{E_{Th}Z_L}{\sqrt{R_L^2 + (X_L + X_{Th})^2}} = \frac{E_{Th}Z_L}{\sqrt{R_L^2 + X_{total}^2}} \tag{7}$$

Solving (7) for X_{total} yields two solutions with equal magnitude

$$|X_{total}| = |X_L + X_{Th}| = \sqrt{\frac{E_{Th}^2 Z_L^2}{V_L^2} - R_L^2} \tag{8}$$

Thus, the following steps can be used to identify the sign of β, for every new two consecutive measurements i and $i-1$:

1) Compute $\Delta X_{total} = \left|X_{total}^{i}\right|^2 - \left|X_{total}^{i-1}\right|^2$ using (8).
2) Compute $\Delta X_L = \left|X_L^{i}\right| - \left|X_L^{i-1}\right|$.
3) If $X_L^{i-1} \geq 0$, then β is positive.
4) Else,
5) If $X_L^{i-1} < 0$, and $|\Delta X_L| \langle \varepsilon_\beta$, skip to the next measurement.
6) Otherwise,
7) If $X_L^{i-1} < 0$, check the following conditions:
8) If $\Delta X_L \cdot \Delta X_{total} > 0$, then β is negative.
9) Else if, $\Delta X_L \cdot \Delta X_{total} < 0$, then β is positive.

where ε_β is the minimum variation between the two consecutive measurements required for the load reactance to check the sign of β, in order to decrease noise influence.

By monitoring this behaviour, it is possible to identify the sign of β for every new pair of measurements.

For expression (8) to properly identify the sign of β, the chosen value for E_{Th} should be contained in a feasible range, i.e., between $E_{Th}^{\min}$ and $E_{Th}^{\max}$ (5). However, when the load is capacitive and $\beta < 0$, the maximum voltage is not the same as it is when the load is capacitive with $\beta > 0$, or when the load is inductive. In addition, for capacitive load E_{Th} may be smaller than V_L. As a result, the following proposition need to be checked:

$$E_{Th}^{\max} = \begin{cases} V_L, & \text{if } \beta \leq 0 \\ V_L\sqrt{2\sin\theta + 2}, & \text{if } \beta > 0 \end{cases}, E_{Th}^{\min} = \begin{cases} V_L, & \text{if } \theta \geq 0 \\ V_L\cos\theta, & \text{if } \theta < 0 \end{cases} \tag{9}$$

2.5. Proper computation of the equivalent active and reactive power

If a bus with PMU measurements has multiple branches (transmission lines, transformers, loads) connected to it, as shown in Fig. 6, a special approach must be employed to correctly calculate the equivalent active and reactive power. The proposed idea is to combine the complex power flows from branches that have active power entering the bus or to combine the complex power flows from branches which active powers are leaving the bus:

$$\overline{S}_L = \sum_{i=1}^{m}(P_i + jQ_i) = \sum_{i=m+1}^{m+n}(P_i + jQ_i) \tag{10}$$

where m is the number of branches with active power flow entering the measurement bus, and n is the number of branches with active power flow exiting the measured bus. The following expressions make the bus in Fig. 6 to be equivalent to the bus in Fig. 3:

$$\overline{V}_L = \overline{V}, \overline{I}_L = \left(\frac{\overline{S}_L}{\overline{V}_L}\right)^* \tag{11}$$

The obtained $\overline{V}_L$ and $\overline{I}_L$ are used to estimate Thévenin parameters.

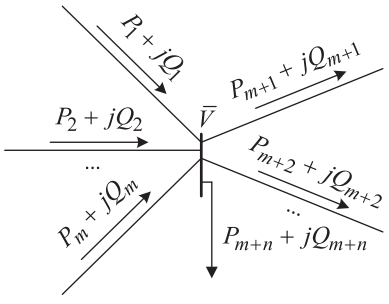

Fig. 6. Power flows entering and exiting a measurement bus.

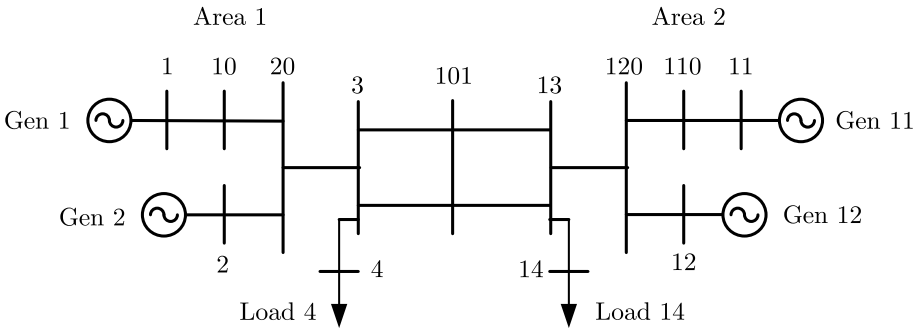

Fig. 7. The Kundur 2-area system.

2.6. Algorithm of the proposed extended adaptive approach

The formulations described in Sections 2.2 – 2.5 are combined to establish the following algorithm:

1) Set the two correction constants k_1 and k_2, where $k_1 > k_2$, and the threshold constant k_b.
2) Measure two consecutive loading conditions (V_L^i, I_L^i) and (V_L^{i-1}, I_L^{i-1}), and compute $E_{Th}^{\min}$ using (9).
3) Identify the sign of β using the approach in Section 2.4, set $E_{Th} = E_{Th}^{\min}$ in (8), and compute $E_{Th}^{\max}$ using (9).
4) If $i = 1$, compute $E_{Th}^0 = E_{Th}^{avg}$, using (5) and (9),
5) Set $E_{aux} = E_{th}^{i-1}$.
6) Compute X^i from (V_L^{i-1}, I_L^{i-1}), X_{pert}^i from (V_L^i, I_L^i), using (3), (4) and E_{aux}, then $\Delta X_{Th} = X_{pert}^i - X^i$.
7) Compute the increment $\delta E_{Th} = \begin{cases} E_{aux}k_1, & \text{if } \Delta X_{Th} > k_b \\ E_{aux}k_2, & \text{otherwise} \end{cases}$, and then $E_+ = E_{aux} + \delta E_{Th}$ and $E_- = E_{aux} - \delta E_{Th}$.
8) Compute X_+^i from (V_L^{i-1}, I_L^{i-1}), X_{pert+}^i from (V_L^i, I_L^i), using (3), (4) and E_+.
9) Compute X_-^i from (V_L^{i-1}, I_L^{i-1}), X_{pert-}^i from (V_L^i, I_L^i), using (3), (4) and E_-.
10) Compute $\Delta X_{Th+} = X_{pert+}^i - X_+^i$ and $\Delta X_{Th-} = X_{pert-}^i - X_-^i$.
11) Check the following conditions:
    a. If $\Delta X_{Th+} < \Delta X_{Th}$, then set $E_{th}^i = E_+$.
    b. Else, if $\Delta X_{Th-} < \Delta X_{Th}$, then set $E_{th}^i = E_-$.
    c. Else, set $E_{th}^i = E_{th}^{i-1}$.
12) Compute β^i and X_{Th}^i, using (3), (4), and E_{Th}^i.
13) Increment i and go back to step 2.

In this way, the minimization of ΔX_{Th} is pursued, and the smaller the values acquired by this quantity, the closer the Thévenin parameters will be to its convergence.

Besides its ability to properly estimate for all four quadrants in Fig. 2 in real-time, this approach has the additional advantage of having an adaptive correction for E_{th}^i, updated with two proportionality constants k_1 and k_2, which are chosen based on the estimation error ΔX_{Th} in each iteration. The idea is to use k_1 when the estimated Thévenin parameters are far from the actual values, when larger values for ΔX_{Th} will be computed, and k_2 when the estimation gets closer to convergence and ΔX_{Th} is smaller. This feature achieves, faster convergences with less oscillatory response [16], whether from the initial condition as well as when there are sudden topological changes, or overexcitation limiter action. This feature improves the proportional increment k_a employed in the adaptive approach. The values for k_1 and k_2 are supposed to be in the same range proposed in [16], i.e., 0.0001 to 0.001, and k_b is the threshold that defines whether k_1 or k_2 will be chosen.

If the estimation occurs on boundary buses such as in Fig. 3 or Fig. 6, the approach described in Section 2.5 should be employed for the computation of $\overline{V}_L$ and $\overline{I}_L$ in each iteration.

3. Voltage stability margin indexes

For voltage stability assessment we propose two voltage stability margin indexes: the power transfer stability margin (PTSM) that relies on the estimation of Thévenin parameters, an equivalent-based index, and the critical voltage margin (CVM), a data-driven index, which only requires the measurement of current magnitude and active power from the system to be evaluated.

3.1. Power transfer stability margin

The power transfer stability margin (PTSM) is defined as:

$$PTSM = \frac{P_{\max} - P_L}{P_{\max}} = 1 - \frac{2P_L X_{Th}(1 + \sin(\theta))}{E_{Th}^2 \cos(\theta)} \tag{12}$$

where $P_{\max}$ is the maximum power transferable to the load. The expression (12) was simplified from the well-known expression for the maximum power, under the assumption of $R_{Th} = 0$ and θ is constant:

$$P_{\max} = \frac{E_{Th}^2 \cos(\theta)}{2Z_{Th}(1 + \cos(\theta - \varphi))} = \frac{E_{Th}^2 \cos(\theta)}{2X_{Th}(1 + \sin(\theta))} \tag{13}$$

where φ is the Thévenin impedance angle, which is equal to $\pi/2$ when $R_{Th} = 0$.

If there is no active power flow through the bus PTSM is equal to 1. If the maximum power transfer is achieved, PTSM is equal to 0, which means there is no margin, and the operating point is the tip of the nose point of the PV curve. PTSM is the primary index, which shows how stressed the system is for the whole range of operating conditions since it directly reflects an active power margin.

3.2. Critical voltage margin

Denote the critical Thévenin voltage E_{Th}^{cr} as the Thévenin voltage that corresponds to the situation when the squared sending end reactive power ($\overline{E}_{Th}$ side from Fig. 1) is equal for two consecutive measurements

$$\left(Q_S^{i-1}\right)^2 = \left(Q_S^i\right)^2 \tag{14}$$

Under the assumption of $R_{Th} = 0$ there are no active power losses $(P_S = P_L)$ and $Q_S^2 = S_S^2 - P_S^2 = S_S^2 - P_L^2$. Equation (14) can be expressed using E_{Th}^{cr} as

$$\left(E_{Th}^{cr}\right)^2 \left(I_L^{i-1}\right)^2 - \left(P_L^{i-1}\right)^2 = \left(E_{Th}^{cr}\right)^2 \left(I_L^i\right)^2 - \left(P_L^i\right)^2 \tag{15}$$

Solving (15) for E_{Th}^{cr} yields

$$E_{Th}^{cr} = \sqrt{\frac{\left(P_L^i\right)^2 - \left(P_L^{i-1}\right)^2}{\left(I_L^i\right)^2 - \left(I_L^{i-1}\right)^2}} \tag{16}$$

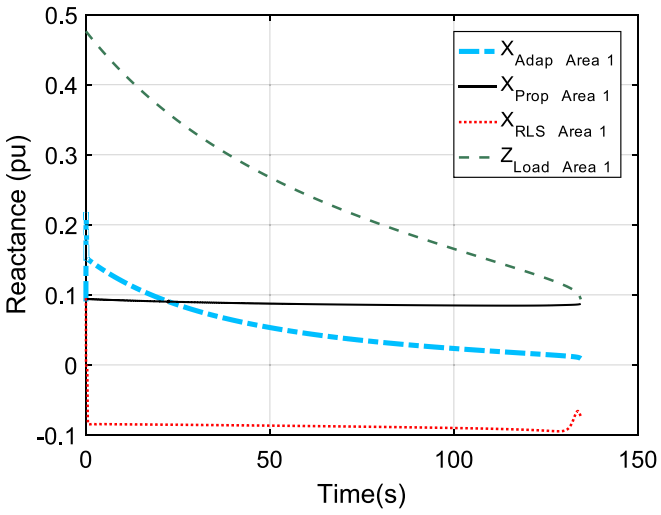

Fig. 8. Thévenin reactance of Area 1.

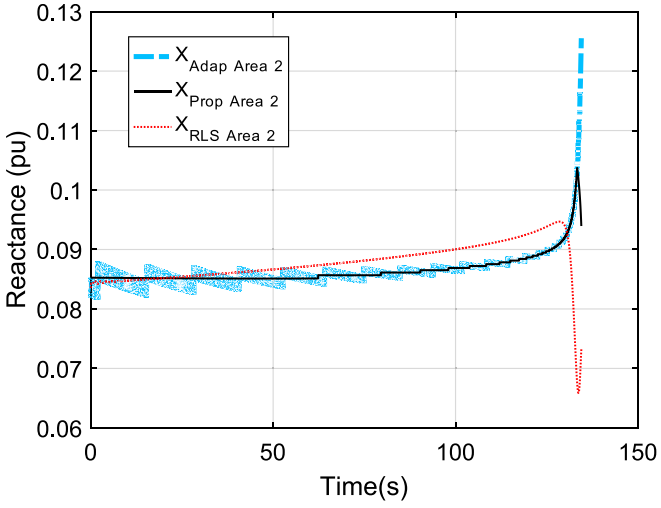

Fig. 9. Thévenin reactance of Area 2.

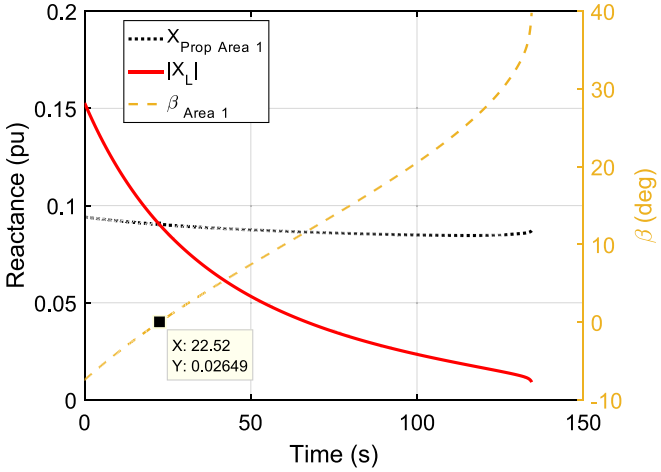

Fig. 10. Relationship between $|X_L|$,X_{Th} andβ.

The critical voltage margin is defined as the squared critical Thévenin voltage

$$CVM = \left(E_{Th}^{cr}\right)^2 = \frac{\left(P_L^i\right)^2 - \left(P_L^{i-1}\right)^2}{\left(I_L^i\right)^2 - \left(I_L^{i-1}\right)^2} \tag{17}$$

The critical Thévenin voltage is squared to avoid complex values for the margin and to allow it to be negative. A positive value of CVM corresponds to the upper portion of the PV curve (before the tip of the noses in Fig. 5), a negative value of CVM corresponds to the lower portion of the PV curve (after the tip of the noses in Fig. 5), and the zero value of CVM corresponds to the maximum power transfer point of the PV curve. The major advantage of this margin index is that it is just based on the PMU measurements and does not require any other information. CVM is the secondary index, which does not directly reflect the active power margin, but is more responsive in comparison to PTSM when the system is closer to the voltage instability inception. Thus, it is useful to compute both: PTSM to track real-time system stressing condition, and CVM to pinpoint the actual voltage instability moment.

4. Case studies

4.1. Kundur 2-area system

To demonstrate the new adaptive approach improvements and its accuracy in estimating the Thévenin parameters, even when the equivalent load is capacitive, i.e., lies in Quadrant 3 or 4 of Fig. 2, the 2-area system [22] is considered (see Fig. 7). Moreover, from this system, it is possible to evaluate the ability of the proposed approach to estimate Thévenin equivalents for both sides with respect to a boundary bus, using the same disturbance data, which is an issue raised by [11,12], where authors mention that approaches based on curve fitting, e.g., based on the least-squares error minimization, are only able to estimate one of the sides, which is called “stable side”.

This system is symmetrical with two generators located in each area. The dynamic data used for this system are found in [23], and the system base power is 100 MVA.

The evaluated scenario represents a positive ramping of power in Load 14, and an equal amount is decreased from Load 4 simultaneously, having for the base case condition the complex powers of $S_{L14} = 8.8 + 0.71$ pu, and $S_{L4} = 3.7 + 0.5$ pu, respectively. This action increases the flow from bus 3 in Area 1 to bus 13 in Area 2 until voltage instability happens. The voltage phasor as well as the active and reactive power are measured at bus 101 (the boundary bus). Those measurements are recorded at a sampling rate of 20 ms and used as PMU measurements.

For this case, as multiple lines are arriving at bus 101, for every new pair of measurements, the equivalent active P_L and reactive Q_L powers need to be computed through the approach described in Section 2.5, before computing the equivalent $\overline{V}_L$ and $\overline{I}_L$ using equation (11).

To show the improvements provided by the proposed approach, two other methods will also be considered, namely the adaptive approach [16] and the recursive least-squares algorithm (RLS) [20].

From Fig. 8, one can verify that the proposed approach converges to a reactance value close to 0.093 pu. The RLS approach converges to an estimated value of -0.085 pu, which is the negative of the Area 2 Thévenin reactance, indicating that Area 1 is the changing side according to [11]. The adaptive approach does not converge to the actual value since the equivalent load is capacitive. For the given scenario, only the proposed approach can properly identify the actual equivalent parameters from Area 1, which shows its robustness against the other presented methods.

For estimating Area 2 parameters, the previously computed load current $\overline{I}_L$ will be reversed, i.e., the considered phasors will be $\overline{V}_L$ and $-\overline{I}_L$.

Fig. 9 shows that the three approaches converge to a value close to 0.085 pu. The positive value of the Thévenin reactance obtained from

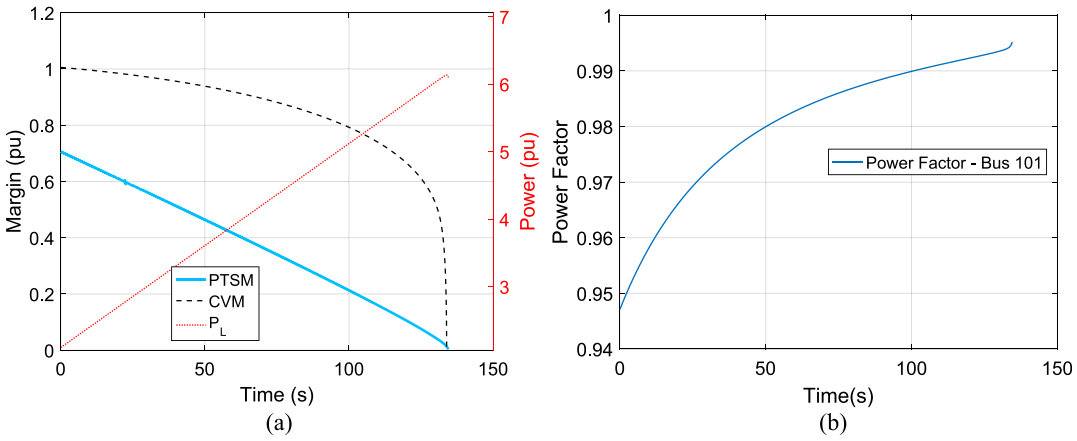

Fig. 11. Voltage instability indexes for the varying power factor case: PTSM and CVM.

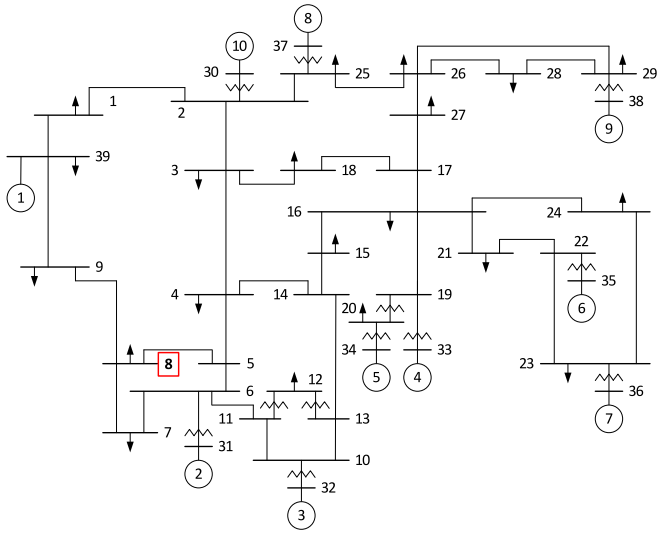

Fig. 12. IEEE 39-bus system.

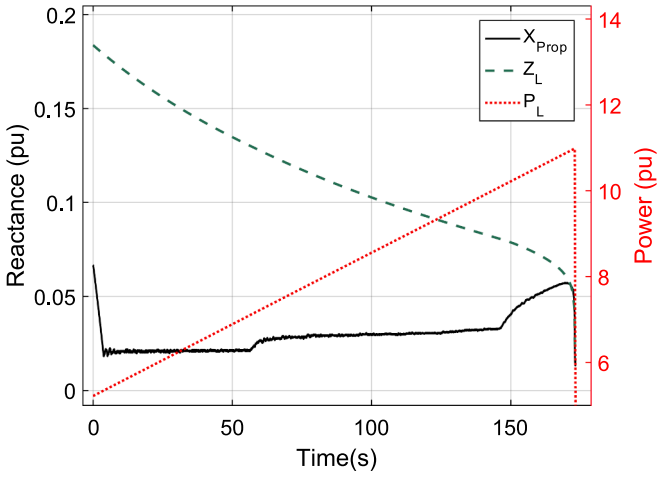

Fig. 13. Estimated Thévenin reactance from bus 8.

the RLS approach reflects that Area 2 is the stable side [11], and the accurate convergence for the adaptive approach occurs because the equivalent load becomes inductive after using $-\bar{I}_L$ instead of $\bar{I}_L$.

Fig. 10 shows the computed β when estimating Area 1 parameters. For this case, the approach in Section 2.4 needs to be employed since the equivalent load has a capacitive characteristic (Quadrant 4 in Fig. 2). One can verify that before 22.5 s, β is negative, and $|X_L| \rangle X_{Th}$. When β becomes positive, which occurs after 22.5 s, $|X_L|$ becomes smaller than X_{Th}, showing the dependence of the β sign on the reactive compensation provided by the load impedance.

The voltage stability margin based on the estimated Thévenin parameters, equation (12), and the margin based only on PMU measurements, equation (17), are shown in Fig. 11(a). One can verify that both move toward zero as the actual power system margin decreases. Because the equivalent load power factor is not constant during the simulation time span (see Fig. 11(b)), PTSM reaches the value of 0 a little later than the maximum power instant. However, CVM reaches 0 exactly at the maximum power transfer point.

For real-world applications, it is practical to set a margin threshold, for example, 0.05 pu, and trigger corrective actions when the margin becomes smaller than the threshold. For both case studies PTSM reaches 0.05 earlier than CVM giving more time for the corrective actions, while CVM provides an accurate estimation of the MPT point. As mentioned in Section 3, utilization of both margins is suggested as it makes voltage stability assessment more robust. Because the margin threshold is a relative quantity, the aforementioned reference value may apply to systems of any size.

4.2. IEEE 39-bus system

To evaluate the proposed approach performance in a larger power system, where voltage instability occurs, considering the existence of non-linear loads and control actions, the well-known New England 39-bus system, representing part of the US Eastern Interconnection network, is considered. The system has 10 generators and is shown in Fig. 12. The scenario of the load increase from [22] is simulated. Loads are modeled as constant power loads. Load 8 is increased by 10 MW/s keeping the power factor constant until voltage instability occurs. The voltage magnitude and angle at bus 8, active and reactive power on lines connected to bus 8 (lines 8–5, 8–7 and 8–9) are recorded at a rate of 30 measurements per second and used as PMU measurements. Equivalent active and reactive power are calculated using (10) and used in the proposed approach to estimate the Thévenin parameters. The estimated Thévenin reactance together with the equivalent load impedance are shown in Fig. 13.

From Fig. 13 one can verify that at about 3.8 s the reactance estimated by the proposed approach (X_{Prop}) converges to the actual value, approximately equal to 0.02 pu, and this is subject to two changes in its value throughout the simulation time span, one at about 60 s and the second one at about 150 s. These changes properly happen since the generators G2 (bus 31) and G3 (bus 32) reach their over-excitation limits

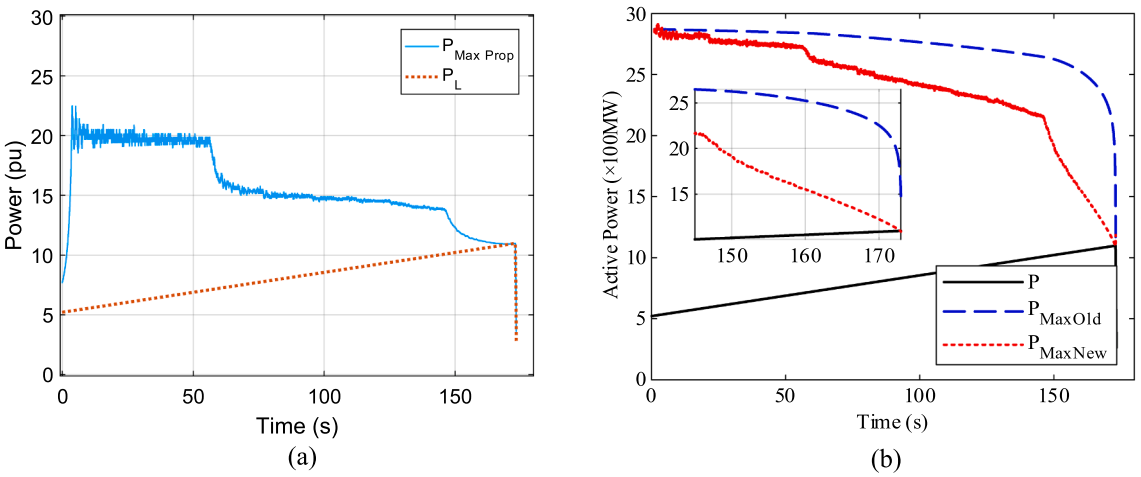

Fig. 14. Comparison of active power limits from [22] and proposed approach.

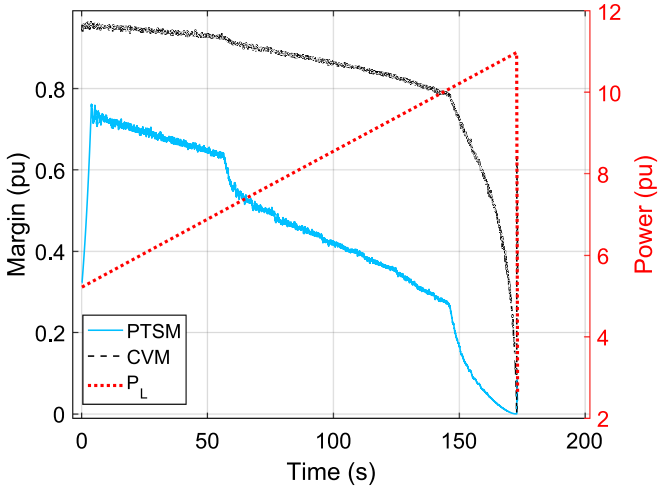

Fig. 15. Voltage instability margins: PTSM and CVM.

just in those times, and accordingly, the actual equivalent reactance from bus 8 increases in each event once those generators lose terminal bus voltage control and the internal machine reactances also become part of the equivalent Thévenin reactance. These updating actions of X_{Prop} reflect that the proposed approach properly responds to the control loop actions from the network.

Fig. 13 also indicates that the estimated Thévenin reactance X_{Prop} properly tracks the MPT, since its impedance matches with Z_L (at 171.5 s) just before the load active power P_L reaches its peak (at 172.9 s).

The accurate performance of the proposed approach is confirmed by Fig. 14(a), showing the equivalent active power P_L, against the maximum power from (13), computed using the estimated equivalent parameters from the proposed method. One can see that at the MPT $P_{Max-Prop} \approx P_L$.

For comparison, Fig. 14(b) extracted from [22], demonstrates the maximum power calculated using the classical Thévenin equivalent approach in [24] (P_{MaxOld}) and the approach in [22](P_{MaxNew}). Maximum powers calculated using approaches in [24] and [22] are far from the actual maximum power (around 11p.u.) for most of the simulation length and only rapidly decrease near the time of voltage collapse. However, the maximum power calculated using the proposed approach in Fig. 14(a), for the given simulation, always provides maximum power estimation values closer to the actual one, in comparison with the approach in [22], Fig. 14(b). Thus, the proposed approach is more sensitive to the changing operating conditions, providing system operators with improved situational awareness.

In addition, PTSM and CVM margins are shown in Fig. 15, and both go towards zero as the system voltage instability approaches, showing the good accuracy of CVM, even not depending on the system parameters as PTSM.

Through this simulation, it is shown the proposed approach can properly track limit induced bifurcation scenarios, e.g., due to over-excitation limiter action as discussed in [22], which were cited in [15] and [7] as circumstances not possible to be tracked by Thévenin equivalent-based approaches for voltage stability analysis. The proposed approach can properly capture system nonlinearities, and hence it is applicable to voltage stability assessment purposes.

5. Conclusions

The proposed extended adaptive approach is able to accurately estimate the Thévenin equivalent parameters seen from any transmission bus, in real-time, regardless in which quadrant of PQ-plane the evaluated PMU measurements lie in and provides accurate parameters estimation of both sides of a measurement bus using the same disturbance data, thus solving the limitations from [16] pointed out in Section 2.2. Consequently, the method accurately tracks the system voltage stability margin through PTSM index, which is based on the Thévenin equivalent parameters, even for limit-induced bifurcation scenarios.

The consistent and reliable performance is achieved through the improvement of the adaptive approach, using a method to properly detect the sign of the Thévenin voltage angle (β) and to properly adapt the Thévenin parameters estimation for each set of two consecutive PMU measurements, correctly updating Thévenin parameters in diverse loading conditions.

Finally, the developed voltage stability margin index based just on PMU measurements, the CVM, has provided accurate results, acting as a relevant complement to the PTSM index in pinpointing the actual MPT, mainly for cases in which the load power factor varies in the evaluated time window.

The proposed approach has been developed for long-term voltage stability assessment purposes. Nonetheless, it can be employed for any other application that requires accurate knowledge of the Thévenin equivalent parameters in real-time as well as in offline analysis.

CRediT authorship contribution statement

Alan P.F. Ferreira: Conceptualization, Methodology, Software, Writing – original draft. **Denis Osipov:** Methodology, Software, Validation, Writing – original draft, Visualization. **Glauco N. Taranto:** Conceptualization, Supervision. **Tatiana M.L. Assis:** Writing – review & editing, Supervision. **Joe H. Chow:** Conceptualization, Writing – review & editing, Supervision.

Declaration of Competing Interest

The authors declare that they have no known competing financial interests or personal relationships that could have appeared to influence the work reported in this paper.

Data availability

Data will be made available on request.

Acknowledgements

This work was supported in part by CNPq, FAPERJ, INERGE, FAPEMIG and Coordenação de Aperfeiçoamento de Pessoal de Nível Superior - Brasil (CAPES) Finance Code 001, and by the Engineering Research Center Program of the NSF and the DOE under the supplement to NSF Award Number EEC-1041877, the CURENT Industry Partnership Program.

Appendix A

A.1. ΔX_{Th} to update Thévenin parameters during estimation

Considering (4) written for an overestimated Thévenin voltage (E_{over}), an underestimated voltage (E_{under}), and its actual value (E_{actual}), for one loading condition. This will yield three expressions for the Thévenin reactance, namely X_{over}, X_{under}, and X_{actual}.

Subtracting X_{over} and X_{under} from X_{actual}, the true deviations between the over and underestimated Thévenin reactance are obtained, respectively, by

$$\Delta X_{over} = \frac{(E_{over}\sin\beta_{over} - E_{actual}\sin\beta_{actual})}{I_L} \tag{A1}$$

$$\Delta X_{under} = \frac{(E_{under}\sin\beta_{under} - E_{actual}\sin\beta_{actual})}{I_L} \tag{A2}$$

As $E_{over} > E_{actual} > E_{under}$, one can verify that $E_{over}\sin\beta_{over} > E_{actual}\sin\beta_{actual} > E_{under}\sin\beta_{under}$. Thus, it is possible to state that the deviations regarding the Thévenin reactance will always have opposite signs in terms of an over- or under-estimated value set for E_{Th}. If β is positive, (A1) is positive and (A2) is negative, and if β is negative, possible for capacitive loads, (A1) becomes negative and (A2) is positive. Moreover, the key information used in the developed algorithm is that the smaller the absolute value computed by (A1) or (A2) yields an estimated E_{Th} closer to the actual value.

In Section 2.5, ΔX_{Th} is computed as the difference between two consecutive estimated X_{Th} (4) from two consecutive loading conditions with E_{Th} constant. Nonetheless, the same pattern regarding the sign is observed, and the minimization of ΔX_{Th} is pursued through the iterations.

A.2. Simplified versus original equations for ΔX_{Th}

The expression (A1) from [16] is employed to quantify the vector error between the estimated ($\bar{E}_{Th}^{est}$) and actual ($\bar{E}_{Th}$) values for the Thévenin equivalent voltage, also described below

$$\Delta\bar{E}_{Th}^{vect} = \bar{E}_{Th}^{est} - \bar{E}_{Th} = j\Delta X_{Th} I_L \tag{A3}$$

where $\Delta X_{Th} = X_{Th}^{est} - X_{Th}$ is the difference between the estimated and actual values for the Thévenin reactance. The phasor diagram in Fig. A1 shows the positions of the actual and estimated Thévenin voltages for the same loading condition $(\bar{V}_L, \bar{I}_L)$, considering an overestimated $\bar{E}_{Th}^{est}$.

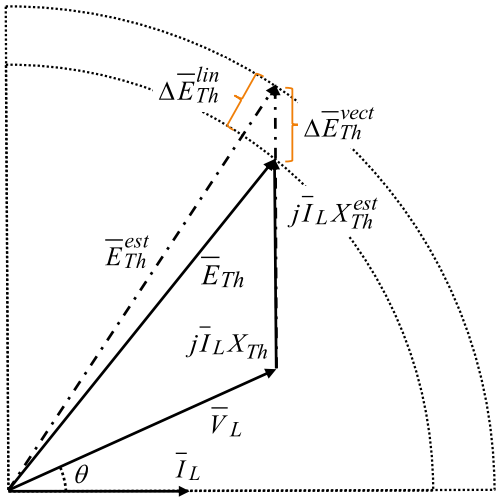

Fig. A1. Diagram showing the actual and estimated Thévenin parameters.

The inner radius represents the vector placement of $\overline{E}_{Th}$, and the outward radius the placement of the overestimated $\overline{E}_{Th}^{est}$.

Using (A3) for two consecutive loading conditions and considering that the estimated voltage $\overline{E}_{Th}^{est}$ magnitude value is kept constant, one can write

$$j\Delta X_{Th}^{i-1} = \frac{\Delta\overline{E}_{Th}^{vect^{i-1}}}{I_L^{i-1}}, j\Delta X_{Th}^{i} = \frac{\Delta\overline{E}_{Th}^{vect^{i}}}{I_L^{i}} \tag{A4}$$

Subtracting the expression in (A4) yields

$$X_{Th}^{est^i} - X_{Th}^{est^{i-1}} = \Delta X_{Th}^{est^i} = \frac{\Delta\overline{E}_{Th}^{vect^{i}}}{I_L^{i}} - \frac{\Delta\overline{E}_{Th}^{vect^{i-1}}}{I_L^{i-1}} \tag{A5}$$

If the error vector is considered constant between the "$i-1$" and "i" measurements, (A5) becomes

$$X_{Th}^{est^i} - X_{Th}^{est^{i-1}} = \Delta X_{Th}^{est^i} = \Delta\overline{E}_{Th}^{vect^{i}} \frac{\left(I_L^{i-1} - I_L^{i}\right)}{I_L^{i} I_L^{i-1}} \tag{A6}$$

Equation (A6) is developed in [16] to state that the difference between the current magnitudes (or between the load impedances) is sufficient to establish the sign on the left side of this equation. Nonetheless, since the error vector magnitude actually is not kept constant when the loading condition is changed, but the error $\Delta\overline{E}_{Th}^{lin}$ (Fig. A1), (A6) is still valid in defining the sign of $\Delta X_{Th}^{est^i}$ when the load variation between "$i-1$" and "i" occurs keeping the load power factor constant. Table A1 shows the right sides (A5) and (A6) computed from Cases 1 and 2 found in Section 2.2.3.

One can verify that the third column of Table A1 is equal to the seventh column of Table 1, showing the high accuracy of (A5) in computing $\Delta X_{Th}^{est^i}$. However, when (A6) is used for Case 1, it will compute a value with a proper sign, even though the value is not accurate. However, for Case 2, when the power factor of the load varies, this expression fails to provide the proper sign, and therefore, the updating decision is no longer correct.

Table A1
Comparing Results from (A5) and (A6).

Case	$E_{Th0}(pu)$	$Equation(A5)(pu)$	$Equation(A6)(pu)$
1	1.0001	−1.92E-05	−4.54E-05
	0.9999	1.92E-04	4.54E-05
2	1.0001	4.69E-05	−9.13E-07
	0.9999	−4.72E-05	9.13E-07

References

[1] ERCOT, "Report on existing and potential electric system constraints and needs," Dec. 2019. [Online]. Available: http://www.ercot.com/content/wcm/lists/172485/2019_Constraints_and_Needs.pdf.

[2] ELECTRIC POWER RESEARCH INSTITUTE (EPRI), "Exploring the Impacts of Extreme Events, Natural Gas Fuel and Other Contingencies on Resource Adequacy," EPRI, California, 2021.

[3] Taylor CW. Power system voltage stability. Singapore: McGraw-Hill; 1994.

[4] van Cutsem T, Vournas C. Voltage stability of electric power systems. Springer Science+Business Media; 1998.

[5] M. Glavic and T. van Cutsem, "A short survey of methods for voltage instability detection," in *IEEE Power and Energy Society General Meeting*, Detroit, MI, 2011.

[6] Mandoulidis P, Vournas C. A PMU-based real-time estimation of voltage stability and margin. Electr Power Syst Res Jan. 2020;178:1–12.

[7] Vournas CD, Lambrou C, Mandoulidis P. Voltage stability monitoring from a transmission bus PMU. IEEE Trans Power Syst Jul. 2017;32(4):3266–74.

[8] Aminifar F, Fotuhi-Firuzabad M, Safdarian A, Davoudi A, Shahidehpour M. Synchrophasor measurement technology in power systems: Panorama and state-of-the-art. IEEE Access Dec. 2014;2:1607–28.

[9] Singh B, Sharma NK, Tiwari AN, Verma KS, Singh S. Applications of phasor measurement units (PMUs) in electric power system networks incorporated with FACTS controllers. International Journal of Engineering, Science and Technology 2011;3(3):64–82.

[10] Chow JH, Sanchez-Gasca JJ. Power System Modeling, Computation, and Control. Wiley-IEEE Press 2020:5–6.

[11] Abdelkader SM, Morrow DJ. Online tracking of Thevenin equivalent parameters using PMU measurements. IEEE Trans Power Syst May 2012;27(2):975–83.

[12] Abdelkader SM, Morrow DJ. Online Thevenin equivalent determination considering system side changes and measurement errors. IEEE Trans Power Syst Sep. 2015;30(5):2716–25.

[13] Kundur P, Paserba J, Ajjarapu V, Andersson G, Bose A, Canizares C, et al. Definition and classification of power system stability. IEEE Trans Power Syst May 2004;19 (2):1387–401.
[14] Liu J-H, Chu C-C. Wide-area measurement-based voltage stability indicators by modified coupled single-port models. IEEE Trans Power Syst Mar. 2014;29(2): 756–64.
[15] Wang Y, Pordanjani IR, Li W, Xu W, Chen T, Vaahedi E, et al. Voltage stability monitoring based on the concept of coupled single-port circuit. IEEE Trans Power Syst Nov. 2011;26(4):2154–63.
[16] Corsi S, Taranto GN. A real-time voltage instability identification algorithm based on local phasor measurements. IEEE Trans Power Syst Aug. 2008;23(3):1271–9.
[17] Smon I, Verbic G, Gubina F. Local voltage-stability index using Tellegen's theorem. IEEE Trans Power Syst Aug. 2006;21(3):1267–75.
[18] Corsi S, Taranto GN. Reliability analysis of voltage instability risk indicator based on a novel real-time identification algorithm. Eur Trans Electr Power 2011;21(4): 1610–28.
[19] G. N. Taranto, C. Oyarce and S. Corsi, "Further investigations on a phasor measurement-based algorithm utilized for voltage stability awareness," in *IREP Symposium Bulk Power System Dynamics and Control - IX Optimization, Security and Control of the Emerging Power Grid*, 2013.
[20] Milosevic B, Begovic M. Voltage-stability protection and control using a wide-area network of phasor measurements. IEEE Trans Power Syst Feb. 2003;18(1):121–7.
[21] C. S. Carvalho and G. N. Taranto, "Comparison of Voltage Instability Identification Methods Based on Synchronized Measurements," in *International Conference on Smart Grid Synchronized Measurements and Analytics (SGSMA)*, 2019.
[22] Liu C, Hu F, Shi D, Zhang X, Sun K, Wang Z. Measurment-Based Voltage Stability Assessment Considering Generator VAR Limits. IEEE Trans Smart Grid 2020;11(1): 301–11.
[23] Kundur P. "Small-Signal Stability". Power System Stability and Control EPRI 1994: 813–4.
[24] Vu K, Begovic MM, Novosel D, Saha MM. Use of local measurements to estimate voltage-stability margin. IEEE Trans Power Syst 1999;14(3):1029–35.